East European Journal of Physics. 3. 456-464 (2024)
DOI:10.26565/2312-4334-2024-3-55 ISSN 2312-4334

PERFORMANCE OPTIMIZATION OF $MgHfS_3$ CHALCOGENIDE PEROVSKITE SOLAR CELLS USING SCAPS-1D

Abdulai M. Feika[a], Muteeu A. Olopade[a,b], Adeyinka D. Adewoyin[b,c]*
[a]*Department of Physics, Fourah Bay College, University of Sierra Leone, Freetown, Sierra Leone*
[b]*Department of Physics, Faculty of Science, University of Lagos, Akoka, Lagos, Nigeria*
[c]*Physics Unit, Distance Learning Institute, University of Lagos, Nigeria*
**Corresponding Author e-mail: dadeyinka@unilag.edu.ng, kingdavidonfire@gmail.com*
Received June 24, 2024; revised August 2, 2024; accepted August 20, 2024

In this work, magnesium hafnium sulfide $MgHfS_3$ perovskite solar cells have been investigated using numerical modelling and simulation. Perovskite solar cells have received increasing recognition owing to their promising light-harvesting properties. The modelling and simulation of $MgHfS_3$ was successfully carried out using the Solar cell capacitance simulator (SCAPS-1D) software. Consequently, this study developed a base model structure of FTO/TiO_2/$MgHfS_3$/Cu_2O/Au and subsequently explored the effect of varying device layer properties such as absorber thickness, total and interface defect densities with a view of optimizing these parameters for better device performance. Simulating the base model gave the performance characteristics of 0.99 V, 25.21 mA/cm^2, 57.59%, and 14.36% which are the open-circuit voltage (V_{oc}), short-circuit current density (J_{sc}), fill factor (FF) and PCE respectively. The optimal absorber thickness was found to be 300 nm and the optimum density of defects for both TiO_2/Absorber interface and Absorber/Cu_2O interface are respectively 10^{10} cm^{-3} and 10^9 cm^{-3}. The obtained optimized PV parameters are V_{oc} = 1.2629 V, J_{sc} = 24.44 mA/cm^2, FF = 89.46% and PCE = 27.61%. Also, it was established that increasing the device temperature beyond 300K enhanced the short circuit current while other performance characteristics gradually declined. The obtained results suggest that chalcogenide $MgHfS_3$ is a potential absorber material candidate for the production of cheap and very efficient environment-friendly perovskite solar cells.
Keywords: *SCAPS-1D, Perovskites, Optimization, $MgHfS_3$, Efficiency*
PACS: 78.20.Bh; 84.60.Jt; 74.62.Dh; 73.25.+i; 89.30.Cc; 41.20.Cv; 61.43.Bn

1. INTRODUCTION

Perovskite solar cells have emerged as a third-generation solar cell for the replacement of conventional mono and polycrystalline silicon cells as well as second-generation cells, which have issues relating to high cost of production, low efficiency and toxicity. Research issues faced today in chemistry and physics surround maximizing efficiency and reducing energy loss in solar cells to enhance the achieve better performance of solar harvesting materials.

Organic-inorganic lead halide hybrid perovskite solar cells (LHPSC) were introduced as a third-generation device to solve issues of high fabrication cost, low efficiency and toxicity attributed to first-generation silicon solar cells and second-generation thin film solar cells and within a very short time, they achieved an exceptional efficiency of 26.1% [1]. Even though they showed high efficiency compared to their silicon-based counterparts, LHPSC faces intrinsic instability problems caused by moisture, heat and other environmental factors. The toxicity of the lead (Pb) in their material structure also poses a problem and this has restricted their commercialization. Hence, there is a need for the pursuit of substitute materials such as chalcogenide perovskites.

Chalcogenide perovskites (CPs) are good, non-toxic and environmentally friendly photovoltaic (PV) materials which emerged as a result of the shortcomings of hybrid perovskites. They possess both the good electrical properties of halides and the good stability of oxides combined. These properties show they can be good absorbers in solar cells. CPs also follow the regular ABX_3 formula for perovskites, where A and B respectively represent group II cations and group IV transition metals, and X for chalcogen anions, originating from the mineral calcium titanate ($CaTiO_3$) [2].

A variety of CP materials like Barium Zirconium Sulphide ($BaZrS_3$) [3], Strontium Zirconium Sulphide ($SrZrS_3$), Calcium Zirconium Sulphide ($CaZrS_3$), Strontium Titanium Sulphide ($SrTiS_3$) and Calcium Strontium Sulphide ($CaSnS_3$) [4] have been subjected to experimental investigations to ascertain their usefulness for solar cell application. It has also been investigated that Barium zirconium sulphide ($BaZrS_3$), Strontium zirconium sulphide ($SrZrS_3$), Barium Hafnium sulphide ($BaHfS_3$), Strontium Hafnium sulphide ($SrHfS_3$), Calcium zirconium sulphide ($CaZrS_3$) and Calcium Hafnium sulphide ($CaHfS_3$) CPs have a perovskite-type structure with ideal bandgap for application in Photovoltaics [5], [6], [7], [8]. Excitonic properties obtained from theoretical research of CPs reveal that their binding energy (E_B) is greater than that of lead-halide-based perovskites. Also, bandgap and absorption coefficient obtained from Spectroscopic Limited Maximum Efficiency (SLME) show that CPs is a very promising solar cell absorber [9].

Recently, Balogun et al., with the use of density functional theory (DFT), investigated the optoelectronic properties of Chalcogenide Magnesium Hafnium Sulfide ($MgHfS_3$) to determine its bandgap, absorption spectra and material-dependent non-radiation recombination losses. They obtained the band gap and absorption coefficient as 1.43 eV, 4.9×10^8 m^{-1} [10]. This study showed that $MgHfS_3$, whose bandgap is almost near the optimum bandgap for single-junction devices can serve as an efficient absorber material for photovoltaics for which this further study is based.

Cite as: A.M. Feika, M.A. Olopade, A.D. Adewoyin, East Eur. J. Phys. 3, 456 (2024), https://doi.org/10.26565/2312-4334-2024-3-55
© A.M. Feika, M.A. Olopade, A.D. Adewoyin, 2024; CC BY 4.0 license

Simulation software such as solar cell capacitance simulator (SCAPS-1D) is most times employed in the exploration of potential single- or multijunction devices to find possible new device structures. It is a one-dimensional simulator that is implemented in the design of thin film solar cell architectures using several layers of semiconductors. The SCAPS software which was created for the study of thin films like CIGS and CdTe type solar cells can simulate solar cell electrical parameters like the current-voltage and quantum efficiency curves among others. Recently, it has been applied to other thin films like CZTS, Perovskites, crystalline silicon cells, amorphous silicon and bulk heterostructures. SCAPS-1D has been used by many groups for the construction of the latest device configurations by using recent absorber materials like Antimony Selenide (Sb_2Se_3), and Antimony Sulfide (Sb_2S_3) [11], [12], [13], [14], Cu_2XSnS_4 (where X means Fe, Mg, Mn, Ni, or Sr) [15], Tungsten Diselenide (WSe_2) [16], Tin Sulphide (SnS)[17] and perovskites materials like ($FAPbI_3$) [18], $CsPbI_3$ [19], $CsPbBr_3$ [20], Cs_2SnI_6 [21], Cs_2TiBr_6 [22], $CsGeI_3$ [23] $Cs_2AuBiCl_6$ [24], and $Cs_4CuSb_2Cl_{12}$ [25]. In most of these studies, the results from their simulations are in tandem with experimental results.

In this research, $MgHfS_3$ is used as solar cell absorber and it is systematically optimized with the aid of SCAPS simulator. Initially, a planar n-i-p CP device structure ($FTO/TiO_2/MgHfS_3/Cu_2O/Au$) is constructed without considering the impact of parasitic resistances. Thereafter, a methodical study of the device operation is done while varying the CP absorber layer thickness, total (N_t) and interfacial (ETL/Absorber and Absorber /HTL) defect densities. We further explored the influence of parasitic resistances; Series resistance (R_s), Shunt resistance (R_{sh}), and working temperature over the final optimized device to assess the performance of prospective Chalcogenide Perovskite solar devices.

2. DEVICE STRUCTURE AND SIMULATION METHODOLOGY

In this work, a one-dimensional n-i-p planar heterojunction perovskite device architecture ($FTO/TiO_2/MgHfS_3/Cu_2O/Au$) is simulated using the SCAPS-1D (version 3.3.10) software which is a one-dimensional simulation software developed by the Department of Electronics and Information systems, Ghent, Belgium, that computes energy bands, concentrations, J-V characteristics, ac characteristics and spectral response using the basic semiconductor equations comprising of Poisson's (1) and Continuity equations for holes (2) and electrons (3) as shown below [26].

$$\frac{d}{dx}\left[\varepsilon(x)\frac{d\psi}{dx}\right] = q[p(x) - n(x) + n_D^+(x) - n_A^-(x) + p_t(x) - n_t(x)] \quad (1)$$

$$\frac{1}{J}\frac{dJ_p}{dx} + R_p(x) - G(x) = 0 \quad (2)$$

$$-\frac{1}{J}\frac{dJ_n}{dx} + R_n(x) - G(x) = 0 \quad (3)$$

Where ε is the permittivity, q is the electron charge, ψ is the electrostatic potential, n and p are both electron and hole concentrations, n_t is the trapped electron, p_t is trapped hole, n_D^+ is the ionized donor-like doping and n_A^- is the ionized acceptor-like doping concentration, $R_n(x)$, $R_p(x)$ are electron and hole recombination rates, $G(x)$ is the generation rate, J_n and J_p are the electron and hole current density. The SCAPS software comes in handy since it can sometimes be risky, time and resource-consuming to design and fabricate a solar cell without numerically simulating it first. Simulation therefore minimizes risk and time and also analyses the cell layers for proper optimization.

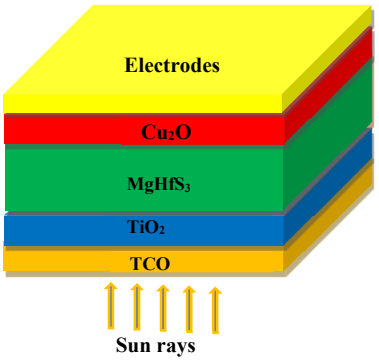

Figure 1. The schematic of n-i-p chalcogenide perovskite solar cell

In this simulation, the absorber layer material used was Magnesium Hafnium Sulfide ($MgHfS_3$) with a bandgap of 1.43 eV. Titanium Dioxide (TiO_2) and Cuprous Oxide (Cu_2O) were used as the electron transport layer (ETL), and as Hole Transport Layer (HTL) respectively. The proposed architecture is shown in Fig. 1 and each simulation was performed using a solar spectrum of one sun AM 1.5 G and 300K working temperature.

Input parameters for all the layers, such as material bandgap, electron and hole mobilities, electron affinity, ETL/Absorber and Absorber/HTL interface defect densities and other input parameters listed in Table 1 and Table 2 respectively are adopted from results of previously published theoretical and experimental work [6], [7], [10], [18], [27], [28], [29]. The optical absorption coefficients of the three layers were obtained by using the square root sub-model of the SCAPS traditional optical model. Also, the thermal velocity of the electron and hole values are inputted as 1×10^7 cm s^{-1}, and the front and back contacts (FTO and Au) work functions are respectively taken as 4.4 eV and 5.1 eV. The influence of parasitic resistances; Series resistance (R_s) and Shunt resistance (R_{sh}), and working temperature over the final optimized device was explored further to investigate the behaviour of prospective Chalcogenide Perovskite-based single-junction devices.

Table 1. Basic device model layer input values

PARAMETERS	FTO (TCO) [30]	TiO_2 (ETL) [27]	$MgHfS_3$ (Absorber) [6], [7], [10]	Cu_2O (HTL) [28]
Thickness (nm)	500	30	500	100
Bandgap (eV)	3.5	3.2	1.43	2.17
Affinity	4	3.9	4.1	3.2
Permittivity	9	9	9.6	7.11
Effective density of states at conduction band	2.2×10^{18}	2.2×10^{18}	2.2×10^{18}	2.02×10^{17}
Effective density of states at valence band	1.8×10^{19}	1.8×10^{19}	1.8×10^{19}	1.1×10^{19}
Electrons mobility	20	20	0.017	200
Holes mobility	10	10	0.059	80
Density of n-type doping	1.0×10^{18}	1.0×10^{19}	1.0×10^{12}	0
Density of p-type doping	0	1	1.0×10^{12}	1.0×10^{18}
Defect density	1.0×10^{15}	1.0×10^{15}	1.0×10^{15}	1.0×10^{15}

Table 2. ETL/Absorber and Absorber/HTL interfacial defects values used in the simulated model

PARAMETERS	ETL/Absorber	Absorber/HTL
Defect type	neutral	Neutral
Capture cross-section e^{-}'s (cm^2)	1.0×10^{-15}	1.0×10^{-18}
Capture cross-section h^{+}'s (cm^2)	1.0×10^{-15}	1.0×10^{-16}
Energetic distribution	Single	Single
Reference for defect energy level (E_t)	Above the highest E_v	Above the highest E_v
Energy with respect to reference (eV)	0.6	0.05
Total defect (cm^{-2})	1.0×10^{11}	1.0×10^{12}

3. RESULTS AND DISCUSSION

Generally, the absorption coefficient(α) of PV material can help determine how the device performs. Fig. 2. shows the SCAPS software-generated absorption coefficient of the three layers (ETL, CP absorber, and HTL layers) as a variation of the energy function.

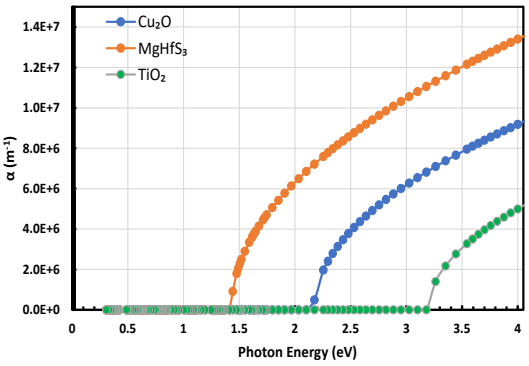

Figure 2. Plot showing the absorption coefficients of Absorber, ETL and HTL layers.

We observed for the absorber, high band-edge values, which confirms the strong light absorption mentioned in previously published theoretical results [10].

The simulation of the basic model device architecture FTO (500 nm)/TiO_2 (30 nm)/$MgHfS_3$ (500 nm)/Cu_2O (100 nm)/Au shown in Fig. 1 was carried out using the SCAPS simulator. The resulting current-voltage characteristics (J-V) graph is shown in Fig. 3a, wherein the major PV parameters like the open-circuit voltage (V_{oc}), short-circuit current density (J_{sc}), fill factor (FF) and PCE are 0.99 V, 25.21 mA/cm^2, 57.59%, 14.36% respectively. The plotted quantum efficiency (QE) graph for the device is displayed in Fig. 3b, where it is observed that the QE enlarged rapidly to the apex of 92% at 360 nm and then decreased to zero at 860 nm. Hence, the optical absorption edge is at 860 nm. Consequently, the QE curve completely covers the entire visible spectrum.

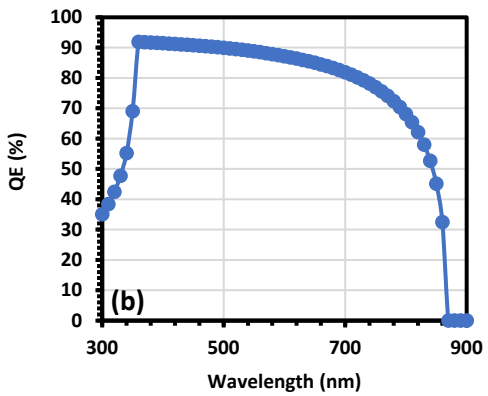

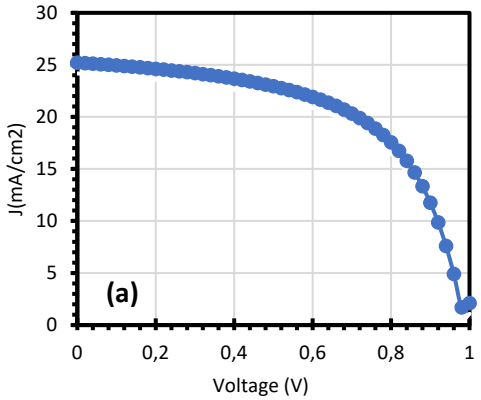

Figure 3. Characteristic J-V curve **(a)** and QE curve **(b)** of the Chalcogenide perovskite device.

3.1 Effect of variation of thickness of Absorber layer

The absorber layer thickness is a key simulation parameter since it plays an important part in the device's operation. The absorber layer must be optimized to absorb a maximum number of photons which in turn leads to the required electron-hole pair generation. Reducing the thickness results in a very close depletion layer resulting in an increment in the recombination rate and consequently decreasing the Power Conversion Efficiency (PCE)[31].

Consequently, the absorber thickness was tuned from 100nm to 600nm, keeping all other parameters constant. Its effect on the device efficiency was studied to establish the optimal absorber layer thickness. It was observed that the device's PCE significantly increased from 11.93% to 16.13% while increasing the absorber thickness from 100 nm to 300 nm and then started decreasing as shown in Figure 4. This can be attributed to the absorber layer thickness greater than the optimal limit, and the charge carrier diffusion length, which results in the creation of higher recombination within the layer. The results denote an optimal thickness of 300nm with a corresponding maximum PCE of 16.13% and a fill factor of 68.58%.

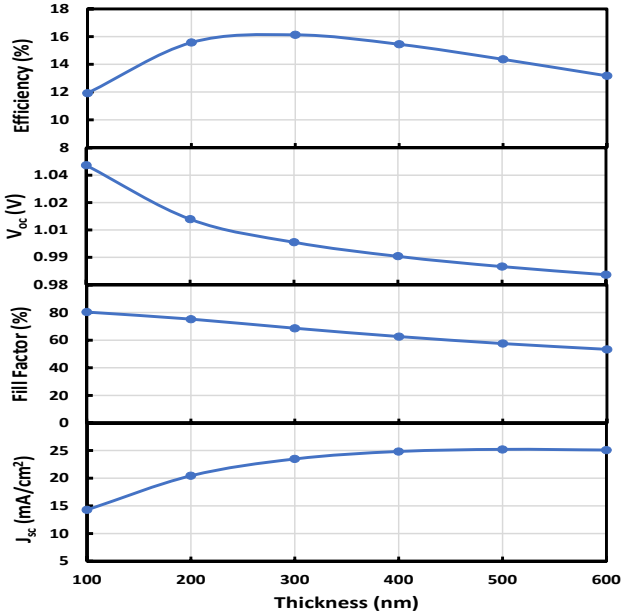

Figure 4. Plot of PV parameters versus absorber layer thickness

3.2 Influence of the Absorber Layer Defect Density

In PSC, the defect density of the absorber hugely affects device performance. The overall performance of the PSC can be reduced for higher absorber defects which can result in higher recombination due to the generation of pinholes and a higher rate of degradation of the film [32], [33]. These defects are mostly at the grain surfaces, interfaces and/or boundaries, as a result of badly organized atoms, dangling bonds, film surface dislocation and poor stoichiometry compositions at grain surfaces [34].

Therefore, a systematic investigation on the effect of the influence of the absorber's defect density on the device's parameters by varying its value from 10 cm^{-3} to 10^{16} cm^{-3} as depicted in Fig. 5. It was observed that there is no significant change in the values of both PCE and V_{oc}, while varying the values from 10 cm^{-3} to 10^5 cm^{-3}. After this, there was a gradual decrement observed, which might be because of higher magnitudes of recombination occurring. However, the FF and J_{sc} values almost remained the same until N_t values increased above 10^{13} cm^{-3}. As the N_t increases, there is a possible reduction in diffusion lengths of electrons and holes [35]. Hence, lower N_t values give excellent performance in the device as a result of the lower rate of recombination in the absorber layer [36].

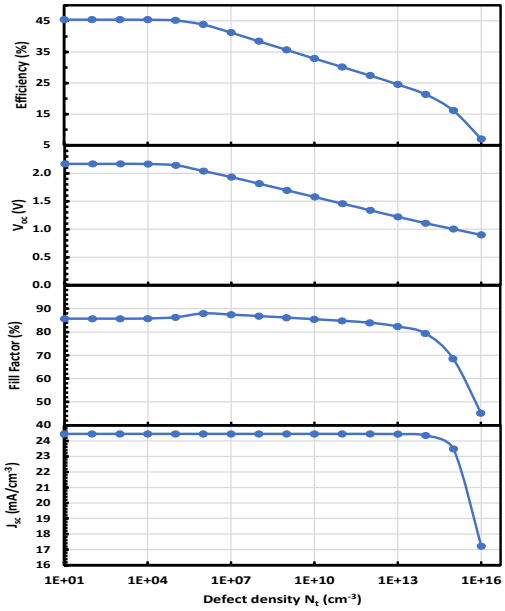

Figure 5. Influence of device PV parameters on absorber defect density.

The optimized defect density value of 10^5 cm^{-3} will be used in the next section to study the influence of the TiO_2/Absorber and Absorber/Cu_2O interface defect densities on the PV.

3.3 Effect of TiO_2/Absorber and Absorber/Cu_2O interfaces defect densities

The processing technique used in producing third-generation solar cells plays a crucial role in their performance. However, interfacial defects are introduced because of structural mismatch. Imperfections in the perovskite/charge extraction layer heterojunctions cause non-radiative losses, which induce V_{oc} loss [37].

In this section, the device performance is further studied by investigating the effect of interfacial defects, such as the TiO_2/Absorber and Absorber/Cu_2O interface defects in the device. The density of the TiO_2/Absorber interface defects is varied from 10^5 to 10^{15} cm^{-3}. The 'localized above the valence band edge (E_v)' defect state was chosen for this simulation.

The effect of the TiO_2/Absorber interface defect density is shown in Fig. 6(a). It is observed that the FF,

V_{oc}, J_{sc} and PCE reduced significantly as the defect density exceeds 10^{10} cm^{-3}. The reduction in defect density is because of the trap-assisted form of recombination occurring at this interface [38]. No significant contribution was noted beyond 10^{10} cm^{-3}, which signifies that a threshold has been reached to ensure optimal device performance.

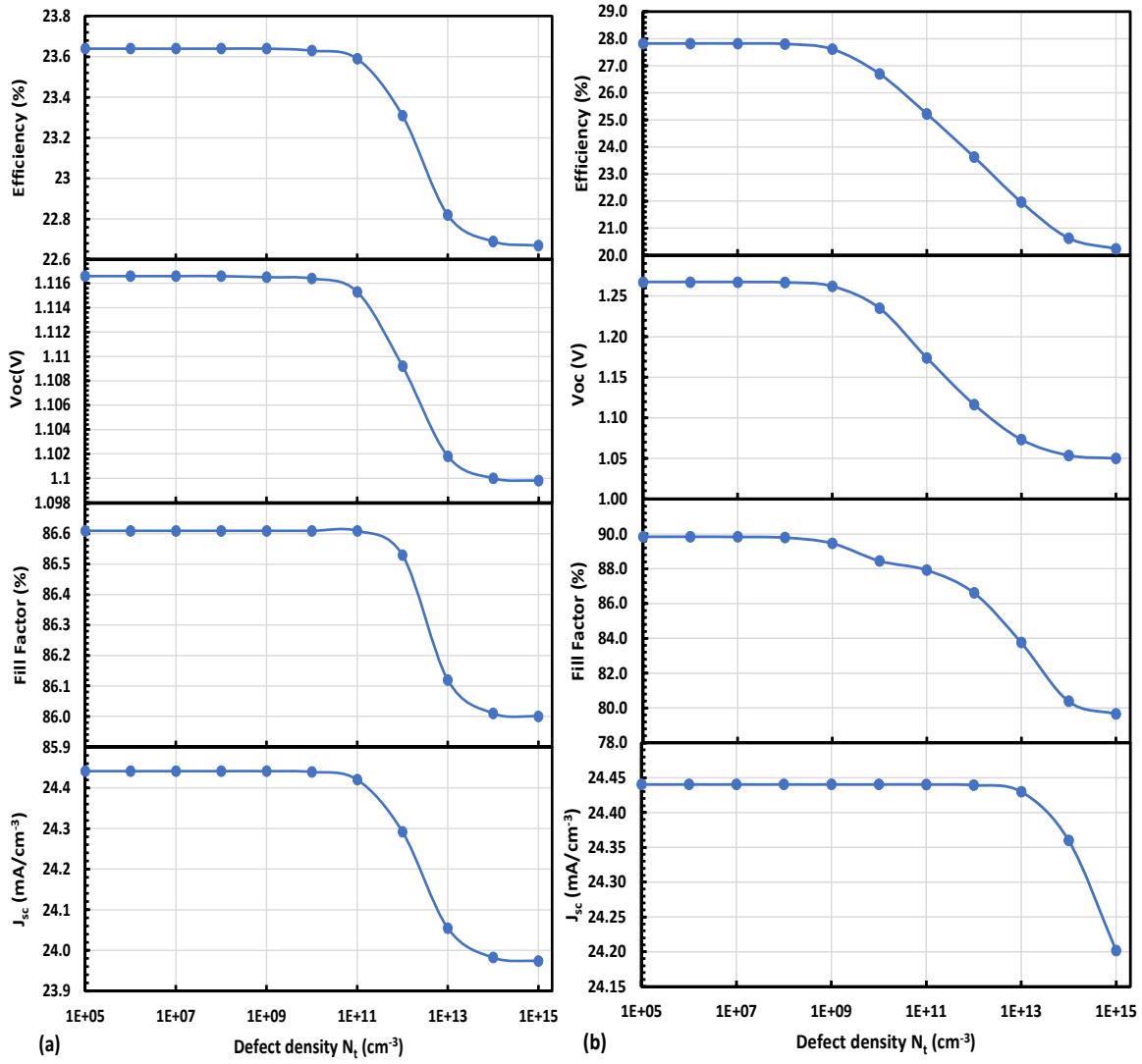

Figure 6. Variation of device PV parameters with defect density at **(a)** TiO_2/Absorber **(b)** Absorber/Cu_2O interface

The defect density for the Absorber/Cu_2O interface was gradually tuned from 10^5 cm^{-3} to 10^{15} cm^{-3} while keeping the other parameters constant as shown in Fig. 6(b). Consequently, the PCE was drastically altered from 27.61% to 20.24% as the defect density goes beyond 10^9 cm^{-3} whilst the J_{sc} reduced drastically with the defect density exceeding 10^{13} cm^{-3}. It was observed that the Absorber/Cu_2O interface has more impact compared to the TiO_2/Absorber interface [39], [40], which may be connected to higher carrier recombination because of the large defect density at the Absorber/Cu_2O interface. Since no crucial changes were observed in the device below the defect density of 10^9 cm^{-3}, the simulated device was considered to be in its optimal performance. It is therefore clear that the increments in the interfacial defect densities particularly influence the V_{oc} and FF instead of the J_{sc}, for both TiO_2/Absorber and Absorber/Cu_2O interfaces, which consequently reduces the performance of the device because of more traps and recombination zones. Therefore, the optimum density of defects for both TiO_2/Absorber interface and Absorber/Cu_2O interface are respectively 10^{10} cm^{-3} and 10^9 cm^{-3}. Hence, the PCE significantly deteriorates beyond these limits.

The optimized basic device layers input parameters, like the absorber thickness and defect density (N_t), and TiO_2/Absorber and Absorber/Cu_2O interfacial defect densities are then incorporated into the device and simulated using these optimum values. Also, the thickness, within the ranges of 30nm to 100nm for the ETL layer and 100nm to 150nm for the HTL layer were tuned respectively to enhance the PV parameters. It was observed that there was no significant contribution of the ETL and HTL layer thicknesses, to the device performance. Therefore, the thicknesses of both ETL and HTL were maintained throughout the simulation. The resulting current-voltage (J-V) characteristics and quantum efficiency of the optimized device is shown in Fig. 7(a) and 7(b) respectively. The obtained optimized PV parameters are V_{oc} = 1.2629 V, J_{sc} = 24.44 mA/cm^2, FF = 89.46% and PCE = 27.61%.

It was however observed that the device performance is enhanced greatly in comparison with the base simulation values. Consequently, the PCE improved from 14.36 % to 27.61 %. The obtained QE graph shown in Fig. 7(b) indicates a major upgrade in the QE compared to the initial simulation values as depicted in Fig. 3(b) and Fig. 7(b). These results of the optimized device depict that the absorber thickness, defect density and Interfacial defect densities play an important part in PV performance enhancement.

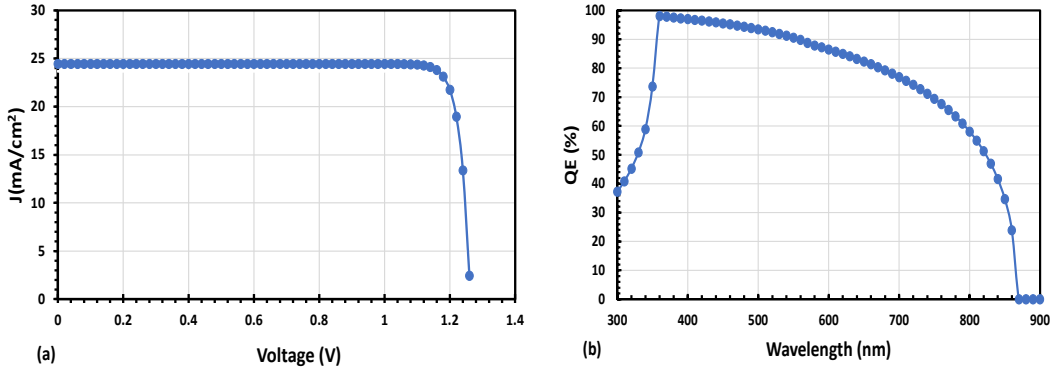

Figure 7. J-V curve (a) and QE curve (b) of optimum CP device.

3.4 Influence of Parasitic Resistances on Device Operation

In actual solar cells, series (R_s) and shunt (R_{sh}) resistances are the main loss mechanisms affecting the performance of the system [18] and they can give a clear impression of how the solar cell operates. Generally, low R_s and higher R_{sh} are associated with high device efficiency. R_s emanates mainly from the reaction of migrated ions from the perovskites layer to the metal contacts thereby restricting charge transfer and resulting in low V_{oc} [41], [42]. R_{sh} is a result of pinholes in the layers or leakage currents caused by manufacturing defects, which in ideal devices cannot be avoided completely but should be kept near the ideal case.

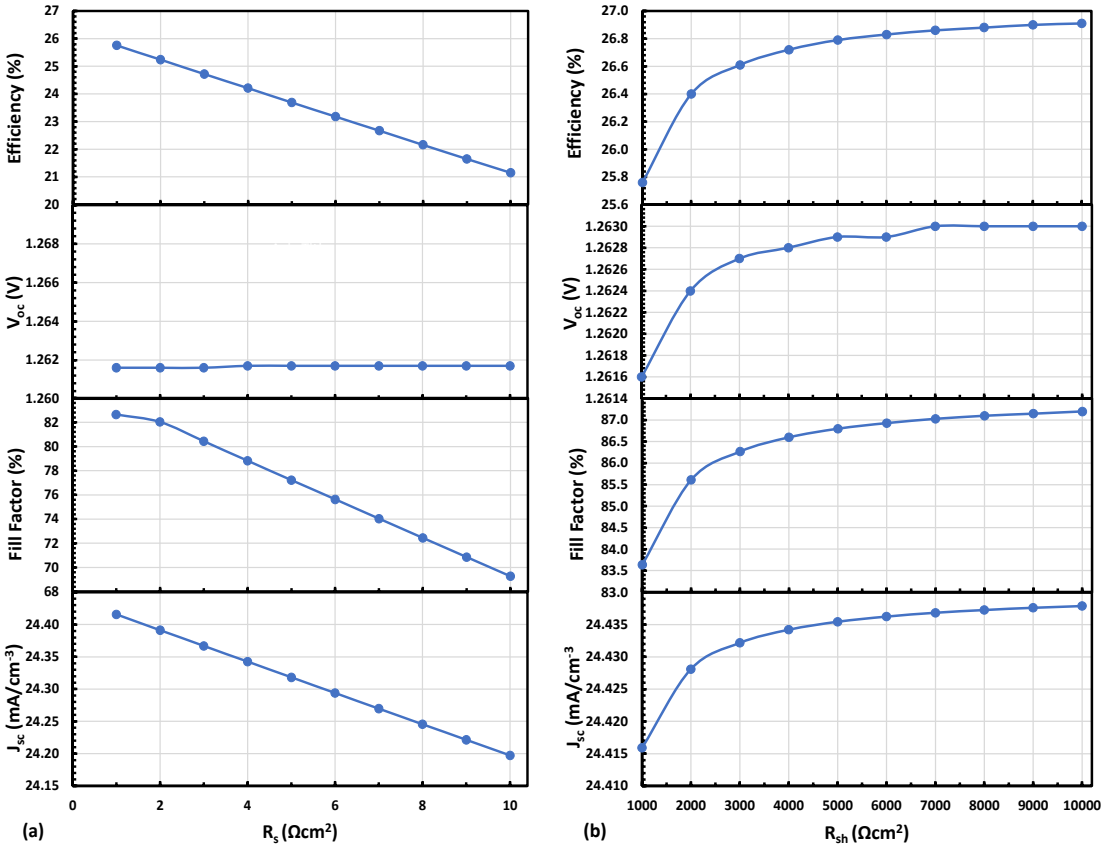

Figure 8. Plots showing the relationship of PV parameters with parasitic resistances, (a) R_s and (b) R_{sh}

In this section, the R_s were varied from 1 Ωcm^2 to 10 Ωcm^2 and R_{sh} from 1000 Ωcm^2 to 10000 Ωcm^2, to better understand how they influence the operation of the optimized device. The resulting graph illustrating the influence of R_s and R_{sh} on the PV parameters is depicted in Fig. 8(a) and (b) respectively. The results indicated that a slight rise in R_s strongly

reduces both the FF and PCE from 82.64 % to 69.25 % and 25.76 % to 21.15 % respectively, as depicted in Fig. 8(a). Also, as illustrated in Fig. 8(b), the FF, Jsc, V_{oc} and PCE rapidly increase with an increment in R_{sh}, with PCE enhancing from 25.76 % to 26.91 %. Therefore, the device performance is improved for higher R_{sh} values. In a real device, solvents and additives are used to enhance morphology behaviour, and passivation substances that perfectly bar shunt pathways are deployed to increase or maintain the R_{sh} value for the effective performance of the device [43], [44], [45], [46].

3.5 Effect of working temperature

Since working temperature has as a significant effect on the operations of the solar cell, temperature values were varied from 300K to 400K under 1 sun constant illumination, while keeping all other simulation input parameters constant. The resulting plot showing the device's PV parameters with different working temperatures is shown in Fig. 9. wherein it was observed that a significant decrease in all PV parameters, except J_{sc}, when the temperature was increased.

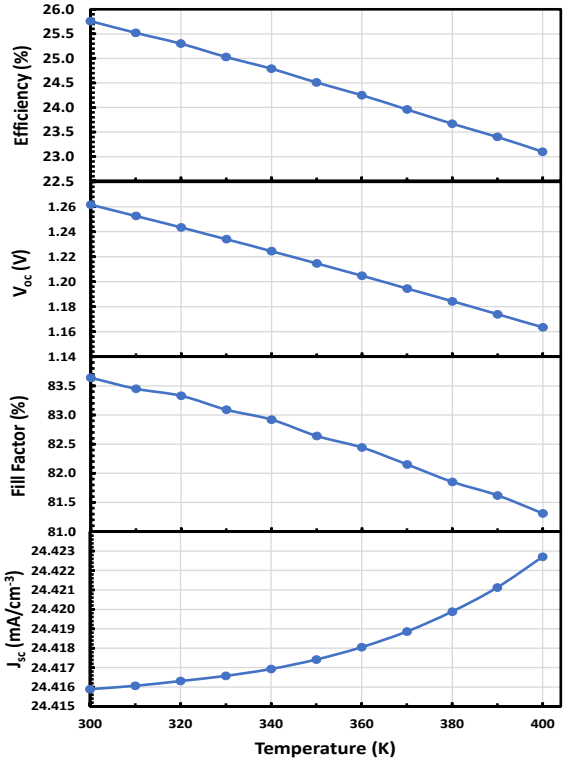

Figure 9. Plot showing the variation of PV parameters with different working temperatures

The V_{oc} behaviour and its temperature dependence can be described by the relation [35], [47].

$$\frac{d}{dT}(V_{oc}) = \frac{V_{oc}}{T} = \frac{E_q/q}{T} \tag{4}$$

Equation (4) shows that an increase in temperature is associated with V_{oc} decrement, which in turn increases the reverse saturation current and a clear decrease in the PCE of the device. The temperature increase may cause some vibrations as a result of thermal excitations, resulting in the recombination of charge carriers [48].

4. CONCLUSION

In this study, we investigated chalcogenide $MgHfS_3$ as an absorber material for solar cells. Consequently, a n-i-p solar cell structure with $MgHfS_3$ perovskite as an absorber layer was systematically modelled and simulated using SCAPS-1D. It was noted that the overall PCE of the PV device baseline model improved from 14.36% to 26.91% through the systematic optimization of the absorber layer thickness, optimum total and interfacial defect densities. The impact on the device performance by parasitic resistances and working temperature was also investigated. There was a reduction in device performance with the introduction of series resistance and increasing working temperature, which provided some ideas on the performance of the device. Our result identifies chalcogenide $MgHfS_3$ as a potential material for the fabrication of cheap but very effective perovskite solar cells. Also, these findings can be helpful for further studies on single-junction chalcogenide perovskite devices.

Acknowledgements

The authors acknowledge Prof. Marc Burgelman and his research group at the University of Ghent for making SCAPS-1D available for our use.

ORCID
Abdulai M. Feika, https://orcid.org/0009-0000-5996-2536; **Muteeu A. Olopade,** https://orcid.org/0000-0002-1126-9027
Adeyinka D. Adewoyin, https://orcid.org/0000-0003-2802-1535

REFERENCES

[1] NREL, "Photovoltaic Research," Interactive Best Research-Cell Efficiency Chart. Accessed: Mar. 01, 2024. [Online]. Available: https://www.nrel.gov/pv/interactive-cell-efficiency.html
[2] D. Tiwari, O.S. Hutter, and G. Longo, "Chalcogenide perovskites for photovoltaics: current status and prospects," J. Phys. Energy, **3**(3), 034010 (2021). https://doi.org/10.1088/2515-7655/abf41c
[3] S. Karthick, S. Velumani, and J. Bouclé, "Chalcogenide $BaZrS_3$ perovskite solar cells: A numerical simulation and analysis using SCAPS-1D," Opt. Mater. **126**, 112250 (2022). https://doi.org/10.1016/j.optmat.2022.112250
[4] H. Shaili, *et al*., "Synthesis of the Sn-based $CaSnS_3$ chalcogenide perovskite thin film as a highly stable photoabsorber for optoelectronic applications," J. Alloys Compd. **851**, 156790 (2021). https://doi.org/10.1016/j.jallcom.2020.156790
[5] Q.A. Akkerman, and L. Manna, "What Defines a Halide Perovskite?," ACS Energy Lett. **5**(2), 604–610 (2020). https://doi.org/10.1021/acsenergylett.0c00039
[6] W. Meng, B. Saparov, F. Hong, J. Wang, D. B. Mitzi, and Y. Yan, "Alloying and Defect Control within Chalcogenide Perovskites for Optimized Photovoltaic Application," Chem. Mater. **28**(3), 821–829 (2016). https://doi.org/10.1021/acs.chemmater.5b04213
[7] Y. Nishigaki, *et al*., "Extraordinary Strong Band-Edge Absorption in Distorted Chalcogenide Perovskites," Sol. RRL, **4**(5), 1900555 (2020). https://doi.org/10.1002/solr.201900555
[8] Y.-Y. Sun, M. L. Agiorgousis, P. Zhang, and S. Zhang, "Chalcogenide Perovskites for Photovoltaics," Nano Lett. **15**(1), 581-585 (2015). https://doi.org/10.1021/nl504046x
[9] M. Kumar, A. Singh, D. Gill, and S. Bhattacharya, "Optoelectronic Properties of Chalcogenide Perovskites by Many-Body Perturbation Theory," J. Phys. Chem. Lett. **12**(22), 5301–5307 (2021). https://doi.org/10.1021/acs.jpclett.1c01034
[10] R.O. Balogun, M.A. Olopade, O.O. Oyebola, and A.D. Adewoyin, "First-principle calculations to investigate structural, electronic and optical properties of $MgHfS_3$," Mater. Sci. Eng. B, **273**, 115405 (2021). https://doi.org/10.1016/j.mseb.2021.115405
[11] I. Gharibshahian, A.A. Orouji, and S. Sharbati, "Alternative buffer layers in Sb_2Se_3 thin-film solar cells to reduce open-circuit voltage offset," Sol. Energy, **202**, 294–303 (2020). https://doi.org/10.1016/j.solener.2020.03.115
[12] V. C. Karade, et al., "Combating open circuit voltage loss in Sb_2Se_3 solar cell with an application of SnS as a back surface field layer," Sol. Energy, **233**, 435–445 (2022). https://doi.org/10.1016/j.solener.2022.01.010
[13] Mamta, K. K. Maurya, and V. N. Singh, "Sb_2Se_3 versus Sb_2S_3 solar cell: A numerical simulation," Sol. Energy, **228**, 540–549, (2021). https://doi.org/10.1016/j.solener.2021.09.080
[14] Mamta, K.K. Maurya, and V.N. Singh, "Enhancing the Performance of an Sb_2Se_3-Based Solar Cell by Dual Buffer Layer," Sustainability, **13**(21), 12320 (2021). https://doi.org/10.3390/su132112320
[15] A. Srivastava, T.R. Lenka, and S. K. Tripathy, "SCAPS-1D Simulations for Comparative Study of Alternative Absorber Materials Cu_2XSnS_4 (X = Fe, Mg, Mn, Ni, Sr) in CZTS-Based Solar Cells," in: *Micro and Nanoelectronics Devices, Circuits and Systems*, **781**, edited by T.R. Lenka, D. Misra, and A. Biswas, (Springer, Singapore, 2022), pp. 329–337. https://doi.org/10.1007/978-981-16-3767-4_31
[16] Md. D. Haque, Md.H. Ali, and A.Z.Md.T. Islam, "Efficiency enhancement of WSe_2 heterojunction solar cell with CuSCN as a hole transport layer: A numerical simulation approach," Sol. Energy, **230**, 528–537 (2021). https://doi.org/10.1016/j.solener.2021.10.054
[17] M. Minbashi, A. Ghobadi, M.H. Ehsani, H.R. Dizaji, and N. Memarian, "Simulation of high efficiency SnS-based solar cells with SCAPS," Sol. Energy, **176**, 520–525 (2018). https://doi.org/10.1016/j.solener.2018.10.058
[18] S. Karthick, S. Velumani, and J. Bouclé, "Experimental and SCAPS simulated formamidinium perovskite solar cells: A comparison of device performance," Sol. Energy, **205**, 349–357 (2020). https://doi.org/10.1016/j.solener.2020.05.041
[19] D. Jayan K, V. Sebastian, and J. Kurian, "Simulation and optimization studies on $CsPbI_3$ based inorganic perovskite solar cells," Sol. Energy, **221**, 99–108 (2021). https://doi.org/10.1016/j.solener.2021.04.030
[20] M. Mehrabian, E.N. Afshar, and S.A. Yousefzadeh, "Simulating the thickness effect of the graphene oxide layer in $CsPbBr_3$ -based solar cells," Mater. Res. Express, **8**(3), 035509 (2021). https://doi.org/10.1088/2053-1591/abf080
[21] A. Chauhan, A. Oudhia, and A.K. Shrivastav, "Analysis of eco-friendly tin-halide Cs_2SnI_6-based perovskite solar cell with all-inorganic charge selective layers," J. Mater. Sci. Mater. Electron. **33**(3), 1670–1685 (2022). https://doi.org/10.1007/s10854-022-07723-x
[22] M.R. Jani, *et al*., "Exploring solar cell performance of inorganic Cs_2TiBr_6 halide double perovskite: A numerical study," Superlattices Microstruct. **146**, 106652 (2020). https://doi.org/10.1016/j.spmi.2020.106652
[23] D. Saikia, J. Bera, A. Betal, and S. Sahu, "Performance evaluation of an all inorganic $CsGeI_3$ based perovskite solar cell by numerical simulation," Opt. Mater. **123**, 111839 (2022). https://doi.org/10.1016/j.optmat.2021.111839
[24] A.J. Kale, R. Chaurasiya, and A. Dixit, "Inorganic Lead-Free $Cs_2AuBiCl_6$ Perovskite Absorber and Cu_2O Hole Transport Material Based Single-Junction Solar Cells with 22.18% Power Conversion Efficiency," Adv. Theory Simul. **4**(3), 2000224 (2021). https://doi.org/10.1002/adts.202000224
[25] Y. He, L. Xu, C. Yang, X. Guo, and S. Li, "Design and Numerical Investigation of a Lead-Free Inorganic Layered Double Perovskite $Cs_4CuSb_2Cl_{12}$ Nanocrystal Solar Cell by SCAPS-1D," Nanomaterials, **11**(9), 2321 (2021). https://doi.org/10.3390/nano11092321
[26] M. Burgelman, P. Nollet, and S. Degrave, "Modelling polycrystalline semiconductor solar cells," Thin Solid Films, **361–362**, 527–532 (2000). https://doi.org/10.1016/S0040-6090(99)00825-1
[27] F. Azri, A. Meftah, N. Sengouga, and A. Meftah, "Electron and hole transport layers optimization by numerical simulation of a perovskite solar cell," Sol. Energy, **181**, 372–378 (2019). https://doi.org/10.1016/j.solener.2019.02.017
[28] S. Karthick, O.M. Nwakanma, B. Mercyrani, J. Bouclé, and S. Velumani, "Efficient 2T $CsKPb(IBr)_3$ Tin Incorporated Narrow Bandgap Perovskite Tandem Solar Cells: A Numerical Study with Current Matching Conditions," Adv. Theory Simul. **4**(11), 2100121 (2021). https://doi.org/10.1002/adts.202100121
[29] V.K. Ravi, *et al*., "Colloidal $BaZrS_3$ chalcogenide perovskite nanocrystals for thin film device fabrication," Nanoscale, **13**(3), 1616–1623 (2021). https://doi.org/10.1039/D0NR08078K

[30] S. Karthick, J. Bouclé, and S. Velumani, "Effect of bismuth iodide (BiI_3) interfacial layer with different HTL's in FAPI based perovskite solar cell – SCAPS-1D study," Sol. Energy, **218**, 157–168 (2021). https://doi.org/10.1016/j.solener.2021.02.041
[31] K. Chakraborty, M.G. Choudhury, and S. Paul, "Numerical study of Cs_2TiX_6 (X = Br−, I−, F− and Cl−) based perovskite solar cell using SCAPS-1D device simulation," Sol. Energy, **194**, 886–892 (2019). https://doi.org/10.1016/j.solener.2019.11.005
[32] M.S. Jamal, *et al*., "Effect of defect density and energy level mismatch on the performance of perovskite solar cells by numerical simulation," Optik, **182**, 1204–1210 (2019). https://doi.org/10.1016/j.ijleo.2018.12.163
[33] G. Xing, *et al*., "Low-temperature solution-processed wavelength-tunable perovskites for lasing," Nat. Mater. **13**(5), 5 (2014). https://doi.org/10.1038/nmat3911
[34] F. Wang, S. Bai, W. Tress, A. Hagfeldt, and F. Gao, "Defects engineering for high-performance perovskite solar cells," Npj Flex. Electron. **2**(1), 22 (2018). https://doi.org/10.1038/s41528-018-0035-z
[35] L. Et-taya, T. Ouslimane, and A. Benami, "Numerical analysis of earth-abundant $Cu_2ZnSn(S_xSe_{1-x})_4$ solar cells based on Spectroscopic Ellipsometry results by using SCAPS-1D," Sol. Energy, **201**, 827–835 (2020). https://doi.org/10.1016/j.solener.2020.03.070
[36] S. Abdelaziz, A. Zekry, A. Shaker, and M. Abouelatta, "Investigating the performance of formamidinium tin-based perovskite solar cell by SCAPS device simulation," Opt. Mater. **101**, 109738 (2020). https://doi.org/10.1016/j.optmat.2020.109738
[37] S. Mahesh, *et al*., "Revealing the origin of voltage loss in mixed-halide perovskite solar cells," Energy Environ. Sci. **13**(1), 258-267 (2020). https://doi.org/10.1039/C9EE02162K
[38] W. Abdelaziz, A. Shaker, M. Abouelatta, and A. Zekry, "Possible efficiency boosting of non-fullerene acceptor solar cell using device simulation," Opt. Mater. **91**, 239–245 (2019). https://doi.org/10.1016/j.optmat.2019.03.023
[39] D. Ompong, and J. Singh, "High open-circuit voltage in perovskite solar cells: The role of hole transport layer," Org. Electron. **63**, 104–108 (2018). https://doi.org/10.1016/j.orgel.2018.09.006
[40] W. Tress, *et al*., "Interpretation and evolution of open-circuit voltage, recombination, ideality factor and subgap defect states during reversible light-soaking and irreversible degradation of perovskite solar cells," Energy Environ. Sci. **11**(1), 151-165 (2018). https://doi.org/10.1039/C7EE02415K
[41] H. Baig, H. Kanda, A.M. Asiri, M.K. Nazeeruddin, and T. Mallick, "Increasing efficiency of perovskite solar cells using low concentrating photovoltaic systems," Sustain. Energy Fuels, 4(2), 528–537 (2020). https://doi.org/10.1039/C9SE00550A
[42] A. Mahapatra, et al., "Changes in the Electrical Characteristics of Perovskite Solar Cells with Aging Time," Molecules, **25**(10), 2299 (2020). https://doi.org/10.3390/molecules25102299
[43] M. Becker, and M. Wark, "Sequentially Deposited Compact and Pinhole-Free Perovskite Layers via Adjusting the Permittivity of the Conversion Solution," Z. Für Naturforschung A, **74**(8), 655–663 (2019). https://doi.org/10.1515/zna-2019-0141
[44] Z. Bi, *et al*., "High Shunt Resistance SnO_2-PbO Electron Transport Layer for Perovskite Solar Cells Used in Low Lighting Applications," Adv. Sustain. Syst. **5**(11), 2100120 (2021). https://doi.org/10.1002/adsu.202100120
[45] D. Saranin, *et al*., "Copper Iodide Interlayer for Improved Charge Extraction and Stability of Inverted Perovskite Solar Cells," Materials, **12**(9), 1406 (2019). https://doi.org/10.3390/ma12091406
[46] R. Singh, S. Sandhu, and J.-J. Lee, "Elucidating the effect of shunt losses on the performance of mesoporous perovskite solar cells," Sol. Energy, **193**, 956–961 (2019). https://doi.org/10.1016/j.solener.2019.10.018
[47] M.A. Green, "General temperature dependence of solar cell performance and implications for device modelling," Prog. Photovolt. Res. Appl. **11**(5), 333–340 (2003). https://doi.org/10.1002/pip.496
[48] Y.H. Khattak, F. Baig, S. Ullah, B. Marí, S. Beg, and H. Ullah, "Enhancement of the conversion efficiency of thin film kesterite solar cell," J. Renew. Sustain. Energy, **10**(3), 033501 (2018). https://doi.org/10.1063/1.5023478

ОПТИМІЗАЦІЯ СОНЯЧНИХ ЕЛЕМЕНТІВ НА ОСНОВІ ХАЛЬКОГЕНІДУ ПЕРОВСКИТУ $MgHfS_3$ З ВИКОРИСТАННЯМ SCAPS-1D

Абдулай М. Фейка[a], Мутеу А. Олопаде[a,b], Адеїнка Д. Адевоїн[b,c]
[a]*Факультет фізики, Коледж Фура-Бей, Університет Сьєрра-Леоне, Фрітаун, Сьєрра-Леоне*
[b]*Кафедра фізики, Факультет природничих наук, Університет Лагосу, Акока, Лагос, Нігерія*
[c]*Відділ фізики, Інститут дистанційного навчання, Університет Лагосу, Нігерія*

У цій роботі перовскітні сонячні батареї магнію-гафнію сульфіду MgHfS3 були досліджені за допомогою чисельного моделювання та моделювання. Перовскітові сонячні батареї отримали все більше визнання завдяки їхнім багатообіцяючим властивостям збору світла. Моделювання MgHfS3 було успішно проведено за допомогою програмного забезпечення моделювання ємності сонячних батарей (SCAPS-1D). В дослідження розроблено структуру базової моделі FTO/TiO_2/$MgHfS_3$/Cu_2O/Au і досліджено вплив змінних властивостей шару пристрою, таких як товщина поглинача, загальна щільність дефектів і щільність дефектів на межі розділу, з метою оптимізації цих параметрів для кращої продуктивності пристрою. Симуляція базової моделі дала робочі характеристики 0,99 В, 25,21 мА/см^2, 57,59% і 14,36%, які є напругою холостого ходу (Voc), щільністю струму короткого замикання (Jsc), коефіцієнтом заповнення (FF) і PCE відповідно. Було встановлено, що оптимальна товщина поглинача становить 300 нм, а оптимальна щільність дефектів як для межі поділу TiO_2/поглинач, так і для межі поглинача/Cu2O становить відповідно 1010 см$^{-3}$ і 109 см$^{-3}$. Отримані оптимізовані параметри PV становлять Voc = 1,2629 В, Jsc = 24,44 мА/см^2, FF = 89,46% і PCE = 27,61%. Крім того, було встановлено, що підвищення температури пристрою понад 300 К посилює струм короткого замикання, тоді як інші характеристики продуктивності поступово знижуються. Отримані результати свідчать про те, що халькогенід $MgHfS_3$ є потенційним кандидатом на поглинач для виробництва дешевих і дуже ефективних екологічно чистих перовскітних сонячних елементів.

Ключові слова: *SCAPS-1D; перовскіти; оптимізація; $MgHfS_3$; ефективність*